Understanding the Dynamics of Mechanically Interlocked Molecular Systems via Metadynamics Simulations

*The Chemical Record*

THE CHEMICAL RECORD
A Journal of the Chemical Society of Japan

REVIEW OPEN ACCESS

# Understanding the Dynamics of Mechanically Interlocked Molecular Systems via Metadynamics Simulations

Clara Sabrià[1] | Luigi Leanza[2] | Massimo Delle Piane[2] | Max von Delius[3] | Ferran Feixas[1] | Xavi Ribas[1] | Giovanni M. Pavan[2]

[1]Institut de Química Computacional i Catàlisi, Universitat de Girona, Girona, Catalonia, Spain | [2]Department of Applied Science and Technology, Politecnico di Torino, Torino, Italy | [3]Institute of Organic Chemistry and Integrated Center of Quantum Science and Technology (IQST), Ulm University, Ulm, Germany

**Correspondence:** Xavi Ribas (xavi.ribas@udg.edu) | Giovanni M. Pavan (giovanni.pavan@polito.it)

**Received:** 29 May 2026 | **Revised:** 11 July 2026 | **Accepted:** 6 August 2026

**Keywords:** catenanes | MD simulations | metadynamics | rotaxanes | WT-metaD

## ABSTRACT

Mechanically interlocked molecules, such as rotaxanes and catenanes, display complex internal dynamics and reciprocal motions that are central to their use as artificial molecular machines. Revealing how these motions occur, the key interactions, and the rate-limiting steps determining their kinetics is essential for understanding and designing functional systems. However, due to scale-, space-, and time-resolution limits, this is typically not easy to access via experimental techniques. In this Personal Account, we discuss representative examples from our recent work using classical molecular dynamics and metadynamics simulations to investigate the key mechanisms, the thermodynamics, and kinetics of the internal dynamics of rotaxanes and catenanes. This allows access to the dynamics of mechanically interlocked systems at atomistic resolution, disentangling bound, unbound, and intermediate states and the dynamical interconversion between them, and providing information on kinetic barriers and characteristic timescales. Such atomistic-scale simulations provide results that are reliable and in very good agreement with the available experimental measurements. Overall, this account illustrates the value of molecular simulations as a predictive and complementary tool for understanding mechanically interlocked molecules in motion.

## 1 | Introduction

Mechanically interlocked molecules (MIMs), such as rotaxanes and catenanes, consist of multiple molecular subparts that are mechanically (but not chemically) linked together, in such a way that separating them requires breaking the covalent framework of at least one of the interlocked constituents. In [n]rotaxanes, one or more macrocycles are locked onto a linear component, called a thread, which has bulky substituents at its ends, called stoppers, that prevent dissociation (Figure 1). The first synthesis was reported by Harrison in 1967 [1]. On the other hand, [n]catenanes feature two or more entangled macrocycles, forming an interlocked chain (Figure 1c). The first examples of the synthesis of catenanes were reported by Wasserman [2] and Schill in the 1960s [3].

The mechanical bond is inherently dynamic, since it allows one component to move with respect to the other [4]. Such internal mobility is one of the defining features of MIMs and underlies their relevance as prototypes of artificial molecular machines (AMMs) [5–9]. The dynamics of these systems can be approximated as two main motions: linear motion, called shuttling, and rotational motion of the macrocycle along/around the thread (Figure 1b). During the last few years, many researchers have tried to design and synthesize AMMs with controllable motion, mimicking nature's machinery. The controlled translational and

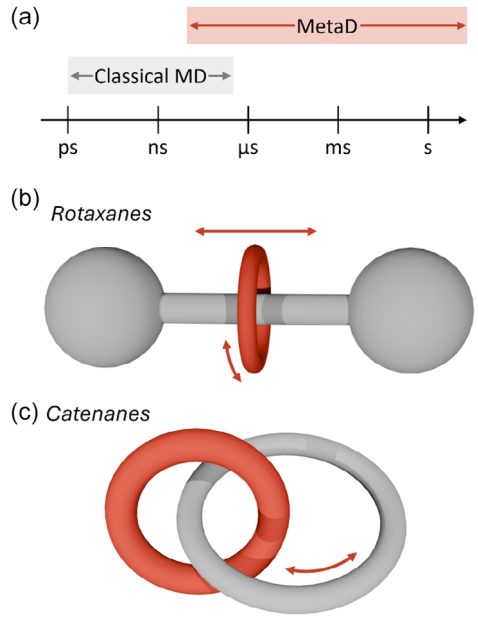


**FIGURE 1** | (a) Timescales achieved for computational techniques like classical molecular dynamics (MD) simulations and metadynamics (MetaD). (b) Schematic representation of a rotaxane with the dynamic motions (shuttling and rotation) indicated with an arrow. (c) Schematic representation of a [2]catenane with the dynamic motion indicated with an arrow.

rotational motions of MIMs are not only of fundamental interest but also constitute the basis for numerous functional applications. By coupling these well-defined molecular motions to external stimuli such as light, redox processes, pH, or chemical fuels, rotaxanes and catenanes have been developed as molecular switches, artificial molecular machines, molecular pumps, and transport systems [7, 10–12]. More recently, these dynamic properties have been exploited in the design of stimuli-responsive materials, adaptive supramolecular assemblies, switchable catalysts, and molecular information storage devices [13–16].

Understanding the free-energy landscape governing these conformational transitions is therefore essential for establishing structure–function relationships and for the rational design of next-generation molecular machines. In this context, atomistic simulations and enhanced sampling techniques such as metadynamics provide unique mechanistic insight into the pathways, intermediates, and energetic barriers associated with these molecular motions. Understanding the dynamics of these systems in realistic conditions of temperature and solvent, and the underlying thermodynamic and kinetic features, is essential for designing MIMs with controlled properties. One important approach to synthesize these molecules is going through a template-assisted synthesis, which involves the interaction of at least one region of one component with the second one [17, 18].

Disentangling all dynamical processes controlling the dynamics of MIMs remains experimentally very challenging. Techniques such as nuclear magnetic resonance (i.e., variable-temperature NMR (VT-NMR) and EXSY experiments) [19–22], or cyclic voltammetry [23] can provide valuable kinetic information. Also, more sophisticated approaches have been applied to extract information on the shuttling dynamics of MIMs, such as time-resolved vibrational spectroscopy [24], optical tweezers [25, 26], and atomic force microscope (AFM)-based force spectroscopy [27]. These techniques do not always resolve the underlying molecular mechanism or identify the rate-determining step directly. For this reason, complementary computational methods are needed to analyze the internal dynamics of these systems at atomistic level.

Molecular simulation methods, such as e.g., all-atom classical molecular dynamics (MD) and metadynamics simulations, may be very useful to this end, allowing to obtain atomistic-scale details of the dynamical behavior of such interlocked systems that are difficult to attain otherwise [28–33]. In this Personal Account, we discuss a series of examples from our recent work in which classical MD and different types of metadynamics (MetaD) simulations (Figure 1a) were combined to investigate the thermodynamics, kinetics, rate-limiting steps, and molecular mechanisms governing the internal dynamic motions in rotaxanes and catenanes. As we will discuss below, for some of these systems, experimental shuttling data are also available, which allow for direct comparison between measured and computed rates. In two such cases, the computed and experimental data were found to be in very good agreement [28, 32], demonstrating the reliability of such computational techniques to access the details of the internal dynamics and dynamical transitions of MIMs. Furthermore, in a recently reported case, the simulations predicted an unusually slow shuttling, on the order of one second, which was later confirmed by VT-NMR experiments [32]. All this reinforces the concept that molecular models and computer simulations are fundamental tools to support the characterization and rational design of complex interlocked molecular systems and to elucidate and even predict their internal dynamical behaviors.

## 2 | Brief Methodological Preface

MD simulations have emerged as a powerful tool for reproducing the motion of molecules at the atomic level [34]. They are used to observe how molecules move and interact with one another, as well as, e.g., to compute/predict their structural, thermodynamic, and dynamic properties. In the last decades, MD has been used to model a variety of systems, from hard to soft matter, from liquids to solids, from synthetic to biologically relevant systems [35–43]. Well-suited to study intermolecular interactions and molecular systems in motion, over the last few years, its application has expanded to other research fields, such as self-assembling systems and supramolecular chemistry [44–52].

To give a very brief introduction, from a theoretical point of view, MD is a simulation method where atoms are treated as particles, and the classical Newtonian equations of motion are solved to describe the dynamics of an atomic/molecular system over time at a given temperature [39, 53–55]. In classical MD, bonded and nonbonded interactions are typically defined by a force field, which defines all bond, angle, and torsional terms, as well as the nonbonded electrostatic and van der Waals terms [56]. Atoms in space are subject to forces originating from the interactions with the other neighbor atoms, which induce over time

atoms/molecules' motions that are resolved in MD simulations in terms of atomic/molecular trajectories. Unlike ab initio approaches, which treat electrons explicitly, this enables the simulation of large molecular systems, typically comprising tens to thousands of atoms, over time scales ranging from picoseconds to microseconds (Figure 1a). While the coarse-grained description granted by such force fields does not allow, on the other hand, for studying phenomena where the electronic state of molecules changes over the simulation (e.g., chemical reactions), in recent years, enormous steps have been made in this sense using deep learning and the training of neural-network potentials based on ab initio calculations [57–63].

Despite these improvements and the access to more precise/reliable force fields, one typical limitation of MD simulations is in the timescales that can be effectively simulated, which typically makes it very difficult to observe and study phenomena occurring on timescales larger than microseconds. To simulate timescales up to milliseconds or more with classical MD, a prohibitively high computational cost is required for systems of practical interest, which in most cases is not affordable. This means that in the case of MIMs, where some transitions/steps in the shuttling dynamics can take up to milliseconds or even seconds, due to the high energy transition barriers separating the metastable states, the internal MIM's dynamics cannot be effectively studied by classical MD simulations (which allow effectively sampling the crossing of low free-energy barriers of up to a few $k_BT$). In such cases where the internal dynamics of MIMs are characterized by higher free energy barriers, it is thus typically necessary to rely on different simulation approaches, such as enhanced sampling simulations.

Among a variety of methods, metadynamics was recently demonstrated to work efficiently for sampling the internal dynamics of MIMs [64, 65]. In brief, metadynamics is an enhanced sampling approach that, thanks to the deposition of a history-dependent free-energy bias, accelerates the crossing of high-free-energy barriers, effectively enhancing the conformational sampling of systems, such as rotaxanes and catenanes (Figure 1) [28, 31, 33, 66]. The method requires choosing one or more collective variables (CVs) that are used to describe the transitions and along which the energy bias is deposited during the simulation to accelerate the escape of the system from local energy minima and the recrossing between the metastable states that might be present [67–70]. The choice of the CVs is a crucial step: a poor CV selection may lead to incorrect estimation of the free energy surface (FES), convergence problems, or even fail to accelerate the dynamics of the studied transition. An ideal well-suited CV should have distinct values in each different metastable state and in the transition state separating them. At the same time, the total number of CVs should remain limited to avoid unnecessary computational cost and convergence problems. Metadynamics also presents some intrinsic limitations, such as the difficulty of reaching and assessing convergence. If the simulation is prolonged excessively, the system may be pushed toward physically unrealistic or irrelevant regions. To mitigate these issues, for example, Well-Tempered Metadynamics have been developed (WT-MetaD) [71], where the bias deposition rate decreases in time (setting up an appropriate bias factor) along the simulation, facilitating, in principle, convergence. At the same time, even such a smoothly converging metadynamics variant has limitations (e.g., a wrong setup of the bias factor may eventually lead to issues related to incomplete sampling, fictitious convergence, etc.). Despite such limitations, this has emerged in recent years as a very well-suited technique to study supramolecular systems, such as MIMs, whose properties are intrinsically interconnected to dynamical transitions and the crossing/recrossing of high free energy barriers. At the same time, the characteristics of MIM systems, supramolecular character, intrinsic dynamics, but relative motions that are intrinsically confined in space and relatively simple to be well described with a low number of CVs, make these systems perfect examples to be studied with metadynamics simulations, which in general (depending on the complexity of the modeled MIM system) allow to estimate free-energy differences between metastable states with good convergence in relatively simple and efficient way.

Another limitation of metadynamics simulations that is worth mentioning is that, in their typical variants, they suffer from limitations in estimating the height of free energy barriers, due to non-negligible bias deposition in correspondence with the barrier during the simulated transitions. To mitigate such limitations and obtain a better estimation of the kinetics for rare events such as the crossing of high free energy barriers, infrequent metadynamics was introduced [68, 72, 73], and in recent years widely used to study molecular transitions/exchange events in supramolecular systems of different kinds [44, 74–78]. In brief, infrequent metadynamics do not require recrossing multiple times between metastable states, but just sampling many times the escape out from one metastable state. By performing multiple simulations, one can build an empirical distribution of escape times, which is fitted with the ideal Poisson distribution expected for rare events. With this, the characteristic timescale of the transition ($\tau$) can be estimated, and from this, the associated transition barrier $\Delta G^{\ddagger}$ can be easily calculated from the Eyring equation [31, 32].

A typical computational workflow consists of initial unbiased classical MD simulations to explore the accessible conformational landscape and identify the slow motions of interest. This information guides the selection of suitable CVs, after which metadynamics are employed to efficiently reconstruct the FES associated with rare events. An illustrative example is shown in Figure 2, where a model rotaxane is represented. In this case, the selected CV is the distance between the macrocycle and point A on the thread. WT-MetaD simulations start from state B. As the bias potential is progressively deposited along the CV, the FES is being filled, which permits the system to reach state B and eventually state C (Figure 2).

The performance of WT-MetaD simulations strongly depends on the choice of the simulation parameters [71, 79]. The bias factor determines the rate at which the deposited bias potential decreases over time and therefore allows the system to freely diffuse over the free-energy landscape and has an important effect on the convergence of the reconstructed FES. Likewise, the Gaussian deposition frequency and the height should be chosen to bias slow transitions without excessively perturbing the underlying dynamics, whereas the Gaussian width should be consistent with the natural fluctuations of the selected CVs. In practice, these parameters are not universal but depend on the characteristic timescales and free-energy barriers of the system under investigation. Their careful selection is therefore

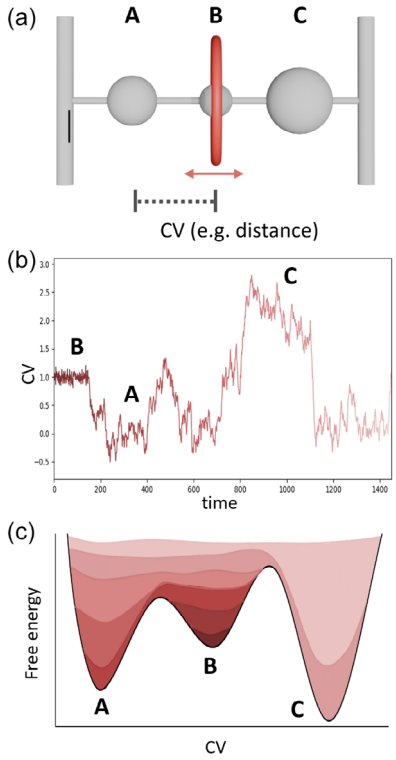


**FIGURE 2** | (a) Representative example of a rotaxane with three binding sites (A, B, and C). Shuttling of the macrocycle between the three states indicated with a red arrow. Description of the CV, being the distance between the geometrical center of the macrocycle and the geometrical center of binding site A. (b) Trajectory of the system as a function of the CV along the simulation time. (c) FES (black line) as a function of the CV. The red-filled area represents the bias potential added to the CV space at different times.

important to achieve efficient sampling while ensuring reliable free-energy estimates.

Clearly, the limitations of metadynamics (the need to preselect a CV, convergence, etc.) make it not as "unbiased and accurate" in sampling transition states and transition kinetics as other methods that may be considered, in principle, more unconstrained (such as transition path sampling, etc.). At the same time, the good match between flexibility, simplicity, efficiency, and accuracy of metadynamics made it well-suited to be applied with success in a variety of scientific fields. Metadynamics-based approaches have been used, for example, to compute the rate of different molecular processes in biology, chemistry, and material sciences. In the supramolecular arena, it has been used to explore the dynamics of guest exchange in-and-out the cavity of a coordination cage [44, 76], molecular exchange events in supramolecular polymers [74, 75], as well as to investigate complex higher-scale supramolecular systems and their emergent properties [78, 80]. Also, metadynamics have been used to gain insight into the assembly process of nanocages [81], or studying guest release [82, 83]. In particular, these have been used with considerable success to explore the dynamics, thermodynamics, and mechanisms of function of interlocked molecular systems, which are central in this account. For example, metadynamics have been used to investigate threading and dethreading mechanisms in pseudorotaxanes, providing atomistic insight into kinetic barriers and transition pathways [84–87].

In the following sections, we discuss representative rotaxane and catenane systems to illustrate how these types of simulations can help understand MIMs, revealing aspects of their behavior that are difficult to obtain with other approaches.

## 3 | Rotaxanes

[n]Rotaxanes consist of a thread or axle that has one or more macrocyclic rings interlocked around it. The nomenclature is such that the letter "n" signifies the total number of components, so a [2]rotaxane comprises one thread and one ring. The stoppers at the end of the thread prevent the dissociation of the two components. The translational movement of the macrocycle along the thread is typically called "shuttling." There is also another important dynamic degree of freedom in these molecules, namely the rotation of the macrocycle. This account focuses only on describing examples of the study of the shuttling, without entering in detail on the macrocycle's rotation. The energy barrier associated with shuttling can depend on the conformational freedom of the thread. If the thread is flexible, it can eventually fold in solution, which can cause a significant increase in the shuttling rate. Some studies have reported that shuttling can be blocked in folded conformations due to steric barriers [88]. In some other cases, flexibility can allow the macrocycle to interact simultaneously with both initial and final recognition sites, which can change the mechanism completely [89]. It is also demonstrated that the length of the thread does not affect the shuttling dynamics in rotaxanes with rigid spacers [90].

The shuttling in simple rotaxanes is controlled by the unbinding of the macrocycle from the recognition site, corresponding to the rate-determining step. Usually, this transition requires the breaking of noncovalent interactions, resulting in a significant energy barrier. For this reason, in the modeling of these systems, we used metadynamics simulations to sample the shuttling transitions and estimate the associated barriers and shuttling rates. In the systems that we discuss herein, once activated (rate-limiting step), the shuttling diffusion along the thread is, in comparison, faster, and in some cases can also be studied through classical MD simulations. Of note, such a hierarchy in the dynamical steps defining the motions of MIMs does not depend only on its structure, but also on surrounding conditions, such as the effect of the external solvent and temperature [28].

In the following sections, four representative [2]rotaxane systems are discussed to illustrate how different structural features influence the shuttling mechanism in terms of thermodynamics and kinetics [28].

### 3.1 | Formamidinium [2]rotaxane

As a first example, a case in which both the thread and the macrocycle are somewhat flexible was considered, namely the minimalistic formamidinium [2]rotaxane (hereafter named **R-1**) reported by Borodin et al. in 2021 [91]. It is formed by an N, N'-disubstituted formamidinium ion and the 24-crown-8 (24C8) macrocycle (Figure 3a). The binding site exists in different configurations, and the *E,Z* and *E,E* isomers can, in

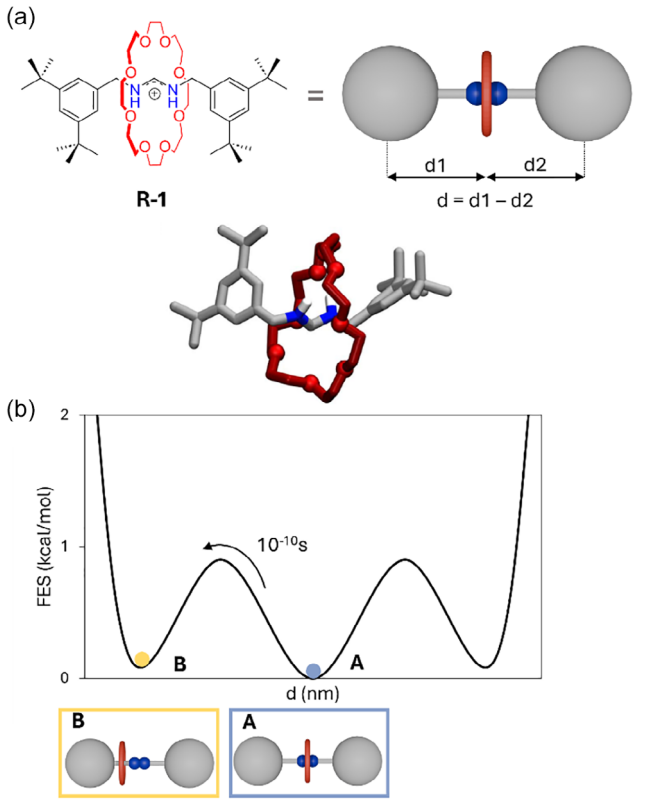


**FIGURE 3** | (a) Structure, schematic representation, and atomistic model of the rotaxane **R-1** [28]. Collective variable (CV) 'd' is the difference in distance between the center of masses of the macrocycle (in red) and each lateral position of the thread. (b) FES as a function of 'd' with the characteristic transition timescales between each state.

principle, interconvert within the timescale of the simulations. This system is a good first representative example since, in this case, the use of metadynamics is unnecessary because the shuttling dynamics are very fast and can be accessed with classical MD simulations.

A single CV was used, which can well describe the position of the 24-crown-8 macrocycle along the thread (d in Figure 3a). The FES can be directly extracted from unbiased MD trajectories by converting the histogram of the probability density (Figure 3b). The most stable structure corresponds to the macrocycle binding the central formamidinium ion in its *E*,*E* configuration. There are also two identical lateral minima when the macrocycle approaches the terminal stoppers. The shuttling takes place at a timescale of 0.1 ns. With this, it can be corroborated that classical MD simulations are a useful method to study dynamics that occur on the nanosecond timescale.

## 3.2 | $[R_4–H_2]^{2+}$ [2]rotaxane

The second system consists of a rigid H-shaped dicationic $[R_4–H_2]^{2+}$ [2]rotaxane (**R-2**) reported by Gholami et al. in 2017 [19]. The rotaxane **R-2** contains two equivalent benzimidazolium recognition sites (in blue) connected through four phenyl rings and a flexible dibenzo[24]crown-8 ether (DB24C8) macrocycle (in red) (Figure 4a). The shuttling rate was determined by EXSY NMR experiments at room temperature, revealing a value of $9.0 \times 10^{-3}\ s^{-1}$, which corresponds to an energetic barrier of 19.8 kcal $mol^{-1}$. With this experimental rate, it can be clearly seen that the shuttling occurs on longer timescales than those

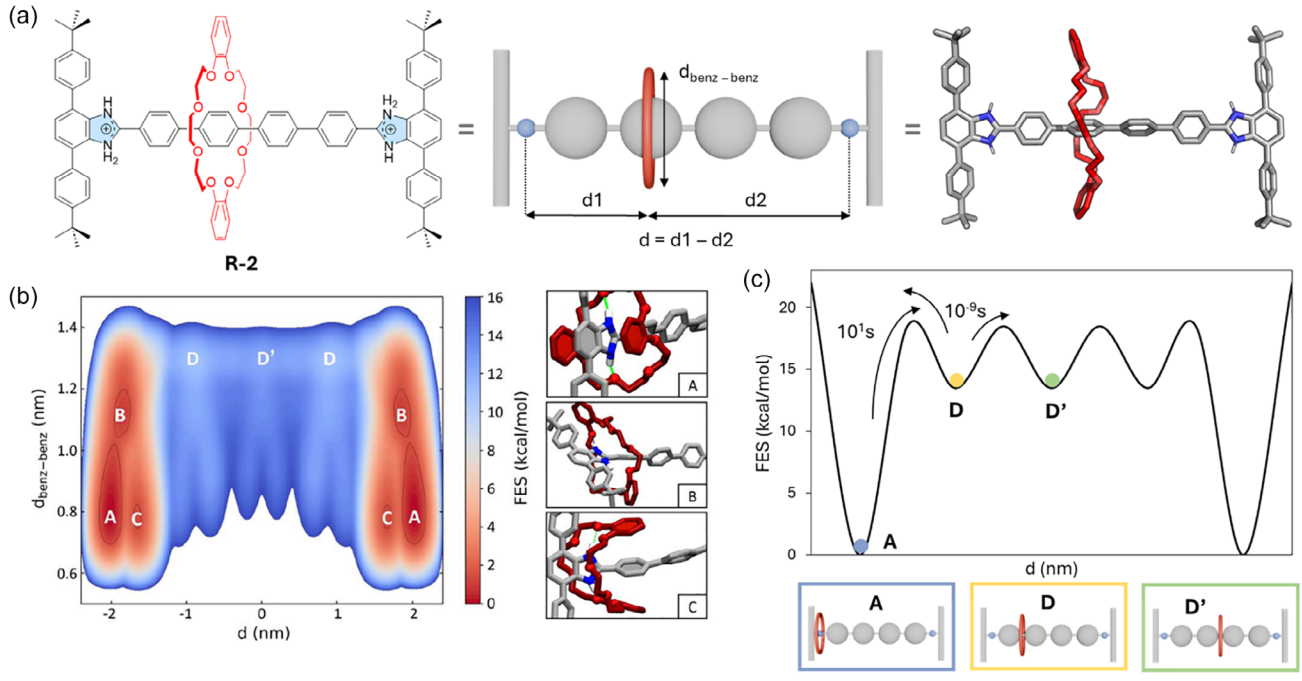


**FIGURE 4** | (a) Structure, schematic representation, and atomistic model of the rotaxane **R-2** [28]. Description of the two CVs: d, being the difference in distance between the center of masses of the macrocycle (in red) and each benzimidazolium recognition site (in blue), and $d_{benz–benz}$, being the distance between the two benzene rings of the macrocycle. (b) FES of the shuttling process as a function of the two CVs (d on the *x*-axis and $d_{benz–benz}$ on the *y*-axis). Snapshots of each state A, B, and C. (c) FES as a function of *d* with the characteristic transition timescales between each state.

that can be measured with classical MD simulations. For this reason, we turned to WT-MetaD simulations.

At first sight, one might expect that a single CV describing the position of the macrocycle along the axle could be sufficient to reconstruct the free-energy profile. But sometimes, more than one CV is needed to do it properly. Here, two different CVs were used: CV1, being the difference in the distance between the geometrical center of the DB24C8 and the center of each recognition site (d), and CV2 being the distance between the two benzene rings of the macrocycle ($d_{benz-benz}$) (Figure 4a). This allowed for better sampling, good convergence, and facile physical interpretation of the obtained data. Looking at the FES (Figure 4b), the macrocycle is more stable when it is located close to the lateral benzimidazolium recognition sites. When the ring is in this bound conformation, three different states (A, B, and C) can be distinguished (Figure 4b), in which *d* presents almost the same value (around 1.5 nm), while $d_{benz-benz}$ differs between states A and C from B. Due to the flexibility of the macrocycle, it can be folded, showing π-stacking of its benzene rings with the phenyl rings of the stoppers (as in state A), or with the central phenyl ring of the thread (as in state C); on the other hand, state B corresponds to the extended macrocycle. Without the use of a second CV, discrimination between these three states would not have been possible. The macrocycle goes to an unbound and intermediate state D, by breaking the hydrogen bonds (H-bonds) between the macrocycle and the benzimidazolium groups on the recognition sites.

The reconstruction of the FES provides a reliable estimation of the free-energy differences ($\Delta G$) between the bound and unbound states. However, to obtain the transition barriers ($\Delta G^{\ddagger}$), infrequent WT-MetaD simulations are needed. In this case, the bound-to-unbound transition is in the order of seconds with an associated transition barrier of ~18.5 ± 0.4 kcal mol$^{-1}$ (Figure 4c), in good agreement, compatible with the precision that can be expected from such classical simulations, with the experimental value extracted from EXSY experiments (19.8 kcal mol$^{-1}$). Such a good agreement supports the kinetic model obtained from the simulations. Compared to the ring unbinding, the shuttling rate along the thread is much faster, with a kinetic barrier of ~6.0 ± 0.3 kcal mol$^{-1}$ and occurring at the nanosecond timescale (Figure 4c).

### 3.3 | Effect of the Solvent in the $[R_4–H_2]^{2+}$ [2]rotaxane

The dynamics of rotaxanes are controlled not only by their structure but also by external conditions, such as the solvent. This statement can be supported by comparing the reconstructed FES for rotaxane **R-2** with three different solvents of different hydrogen-bond donor ($\alpha$) and acceptor ($\beta$) abilities: acetonitrile (MeCN, $\alpha = 0.19$, $\beta = 0.40$), chloroform ($CHCl_3$, $\alpha = 0.44$, $\beta = 0.10$), and dimethyl sulfoxide (DMSO, $\alpha = 0.00$, $\beta = 0.76$) [92]. In this system, the most relevant parameter is the hydrogen-bond acceptor ability $\beta$, because the solvent can compete with the macrocycle by accepting hydrogen bonds from the benzimidazolium recognition site of the thread, which directly affects the dynamics of the rotaxane. Accordingly, DMSO is the strongest hydrogen-bond acceptor,

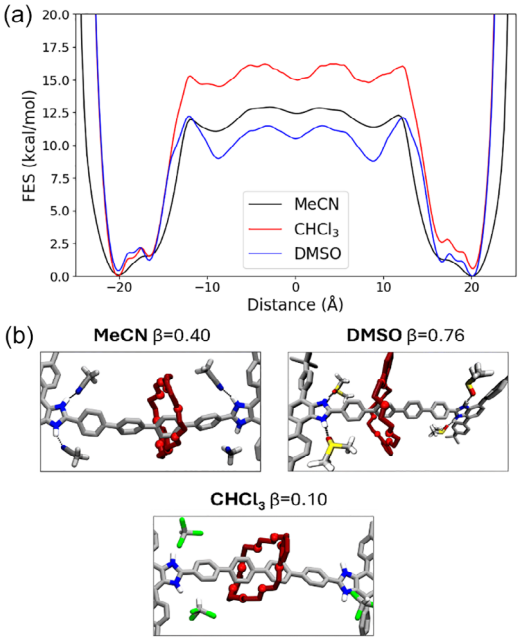


**FIGURE 5** | (a) Comparison of FES for rotaxane **R-2** in MeCN (black), $CHCl_3$ (red), and DMSO (blue) as a function of *d* [28]. (b) Representative snapshot of the unbound state, with the solvent forming hydrogen bonds with the binding site, where applicable.

MeCN is a moderate hydrogen-bond acceptor, and $CHCl_3$ is only weakly competitive (Figure 5b).

The reconstruction of the FES, via WT-MetaD, shows similar results for MeCN and DMSO, while for $CHCl_3$ the barrier is larger (Figure 5a). For $CHCl_3$, the energetic barrier separating the bound and unbound states is ~21.2 ± 0.4 kcal mol$^{-1}$, calculated via infrequent WT-MetaD simulations, being the largest among the three solvents. This is caused by the inability of this solvent to form hydrogen bonds with the benzimidazolium sites. Thus, the shuttling of the macrocycle is less favorable. The barrier is slightly reduced in the MeCN case to ~18.5 ± 0.4 kcal mol$^{-1}$ since the rupture of the hydrogen bonds between the macrocycle and the recognition site is somehow compensated by the formation of hydrogen bonds with the MeCN molecules. The lowest shuttling barrier of ~16.5 ± 0.3 kcal mol$^{-1}$ was found for DMSO, which is likely due to the exceptionally high hydrogen-bond acceptor ability ($\beta$) of this solvent. The correlation of the shuttling barriers with the $\beta$ parameter means that the key process determining relative shuttling kinetics is competition between the solvent and the crown ether for binding the positively charged benzimidazolium site.

### 3.4 | [10]CPP-Fullerene [2]rotaxane

An unusual MIM reported by Xu et al. in 2018 consists of a [10]CPP-fullerene-based [2]rotaxane (**R-3**) [93]. It is formed by a rather rigid macrocycle, the [10]cycloparaphenylene ([10]CPP), and a more flexible thread, which contains a bis-adduct $C_{60}$ in the middle with two bulky $C_{60}$ hexakis-adduct stoppers, separated by two long macrocyclic spacer groups (Figure 6a). Due to the lack of a second binding site, the authors were unable

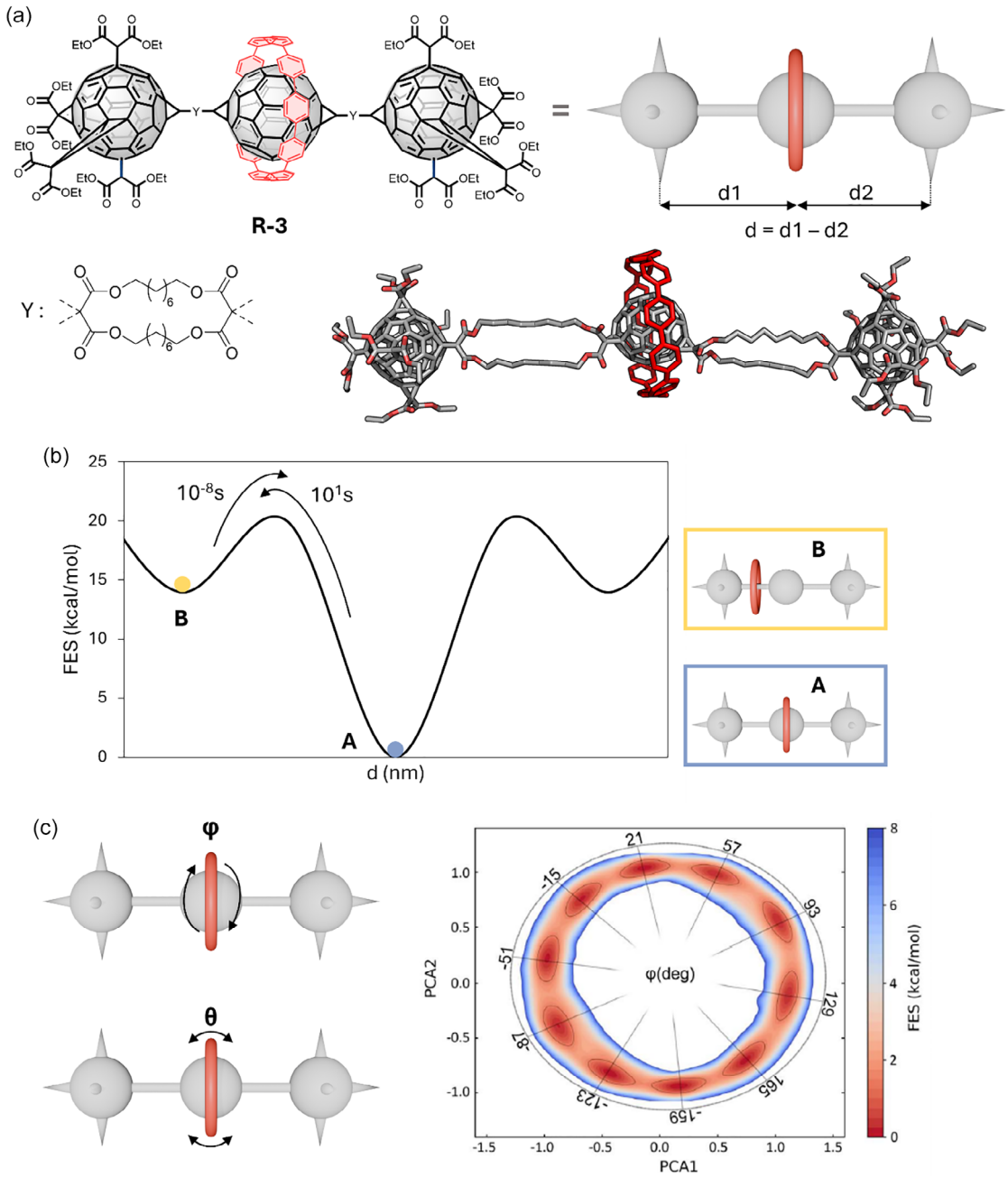


**FIGURE 6** | (a) Structure, schematic representation, and atomistic model of the rotaxane **R-3** [28]. Description of the CV: *d*, being the difference in distance between the center of masses of the [10]CPP nanohoop (in red) and each lateral $C_{60}$ position of the thread. (b) FES as a function of *d* with the characteristic transition timescales between each state. (c) Description of the rotation angle $\varphi$ (top) and tilting angle $\theta$ (bottom) of the [10]CPP around the central $C_{60}$. FES as a function of the [10]CPP angular configurations (sin($\varphi$), cos($\varphi$), sin($\theta$), and cos($\theta$)) projected along the first two PCs.

to directly determine a shuttling rate for this rotaxane **R-3**, but instead they used a pseudorotaxane without one of the stoppers and spacers to calculate the barrier for decomplexation, which can serve as a reasonable proxy for shuttling. By VT-NMR experiments, they obtained an energetic barrier of 13.7 kcal $mol^{-1}$, since the [10]CPP signal splits into two peaks at low temperature due to the deceleration of the complexation/decomplexation equilibrium. They concluded that the dynamic [10]CPP translation in the rotaxane likely occurs roughly on the same millisecond timescale as in the pseudorotaxane. Although the shuttling rate of the rotaxane **R-3** could not be directly determined, the authors observed some NOE signals between the [10]CPP protons and various $CH_2$ groups of the macrocyclic spacer, indicating the existence of translation along the thread. The use of computational methods to extract the shuttling rate between the bound state (when the [10]CPP is interacting with the central fullerene $C_{60}$) and the unbound states (when the [10]CPP is placed on the spacers) is needed in this case, since it could not be obtained experimentally. Also, the timescales are above the ones reachable by classical MD simulations; therefore, WT-MetaD is well-suited to investigate this process.

As detailed above, the thread in this case is flexible. To simplify the analysis and avoid folding effects, the axle was maintained

extended during the simulations by softly restraining the position of the fullerene stoppers. A single CV was chosen, which consists of the difference in distance between the geometrical center of the [10]CPP ring and the center of each lateral fullerene (Figure 6a). Since the macrocycle is rigid, the FES can be reconstructed through a converged WT-MetaD (with a single CV), while the kinetic rates were extracted through multiple infrequent WT-MetaD simulations. The unbinding barrier is in the order of tens of seconds (Figure 6b). Comparing it to the experimental value obtained for the pseudorotaxane, it was concluded that the unbinding of the [10]CPP from a terminal fullerene group (as in the pseudorotaxane) is orders of magnitude faster than the unbinding process in a rotaxane for the [10]CPP to diffuse along the thread. This difference highlights that decomplexation in a truncated host–guest model is not necessarily equivalent to shuttling in the full mechanically interlocked architecture, where the topology and constrained thread geometry can substantially reshape the kinetic barrier. The rotation ($\varphi$) and tilting ($\theta$) of the [10]CPP nanoring around the central fullerene (bound state) were also studied, in this case through classical MD simulations, since it takes place really fast (Figure 6c). A principal components (PC) analysis was carried out over four variables (sin($\varphi$), cos($\varphi$), sin($\theta$), and cos($\theta$)), obtaining the FES as a function of the first two PCs (Figure 6c). It exhibited 10 energetically equivalent minima separated by a transition barrier of ~2 kcal mol$^{-1}$.

### 3.5 | Rigid Bistable [2]rotaxane

The rigid bistable [2]rotaxane (**R-4**) reported by Nygaard et al. in 2007 features two recognition sites [94]. The rotaxane is formed by two naphthalene (NP) recognition sites (in red) that are equivalent and connected through a rigid spacer that simplifies the dynamics (Figure 7a). The ring is the tetracationic macrocycle cyclobis(paraquat-*p*-phenylene) (CBPQT$^{4+}$), known as "blue-box." The shuttling rate in this system was extracted from VT-NMR experiments, obtaining a value of 9.6 ± 0.1 kcal mol$^{-1}$ at a temperature of 199 K.

Again, a single CV was used, being the difference in distance between the center of the blue-box macrocycle and each lateral stopper of the thread (Figure 7a). Through WT-MetaD, the FES was reconstructed (Figure 7b), and the energetic barrier was obtained through infrequent WT-MetaD with a value of ~10–11 kcal mol$^{-1}$, which fits well with the experimental barrier. The characteristic time of the transition going from one station to the other is in the range of $10^{-5}$ s. Also in this case, the computed barrier is consistent with the experimental estimate.

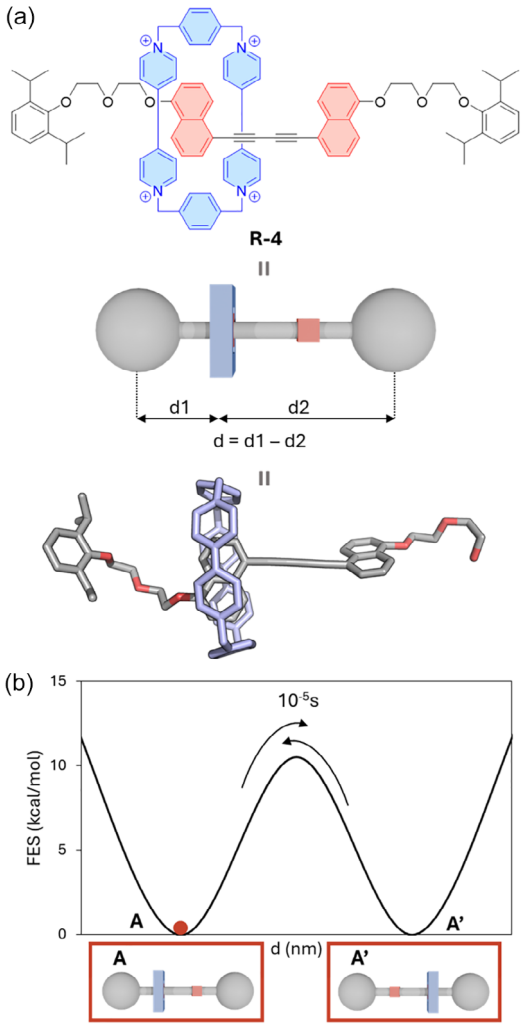


**FIGURE 7** | (a) Structure, schematic representation, and atomistic model of the rotaxane **R-4** [28]. Description of the CV: *d*, being the difference in distance between the center of masses of the blue-box and each lateral position of the thread. (b) FES as a function of *d* with the characteristic transition timescales between each state.

## 4 | Catenanes

As described in the introduction, [n]catenanes consist of two or more entangled macrocycles to give the formation of an interlocked chain, preventing the dissociation of the individual components [95, 96]. Different types of catenanes exist depending on the number of macrocycles present and on how they are entangled with one another. The [2]catenanes consist of only two components, while the [3]catenanes consist of three macrocycles, which can comprise either three identical rings, or two identical macrocycles and one different (as in ABA-type [3]catenanes) [97, 98] or all different (as in ABC-type hetero [3]catenanes). Examples with even five or eight macrocycles have been reported, giving the formation of [5]catenanes [99, 100] and [8]catenanes [101] respectively. A higher degree of catenation can be obtained, such as in poly[n]catenanes [102] and in complex hierarchically self-assembled supramolecular catenanes [66]. However, due to the intermediate self-assembled/interlocked character, in this account, we shall not focus on such more complex systems and focus only on purely mechanically interlocked catenanes.

The dynamics of catenanes can involve the change of the relative positioning of one macrocycle with respect to the other. One macrocycle can have one or more recognition sites, and the shuttling is controlled by the unbinding of the other from one recognition site. The mechanical movement in these kinds of molecules is also directed by noncovalent interactions

between the different components. In most cases, these transitions are slow and cannot be studied using classical MD simulations alone, making enhanced-sampling approaches particularly useful. In the following sections, we discuss two [2]catenanes and one [3]catenane to show how differences in topology and recognition sites affect their dynamics and kinetics.

### 4.1 | $C_{60}$/[10]CPP-Based [2]catenanes

Carbon nanohoops like [n]CPPs have been recently incorporated in MIMs, especially with $C_{60}$-based catenanes and rotaxanes, due to the high affinity between these two molecules as a result of the concave–convex π–π interactions. Two different [2]catenanes containing both the [10]CPP ring as a macrocycle and one or two $C_{60}$ units that act as the recognition sites are studied.

The first example was reported by Steudel et al. in 2023 and consists of a *trans-3* bis-adduct of $C_{60}$ with two malonates connected via alkyl chains and a central bisphenol A (BPA) unit (**C-1** in Figure 8a) [31]. Since the malonates are nonsymmetric bearing two different (ester) substituents, three diastereoisomers (*in*,*in*, *in*,*out*, and *out*,*out*) can be formed. The major product obtained was the *in*,*out-trans-3* isomer, giving the formation of this [2] catenane **C-1** with one single $C_{60}$ recognition site. The unbinding of the [10]CPP from the $C_{60}$ site was studied with infrequent WT-MetaD, since it requires crossing a large free-energy barrier. The predicted characteristic unbinding time in this system is about ~30 s, which corresponds to a $19.3 \pm 0.2$ kcal mol$^{-1}$ kinetic barrier (Figure 8b). This high energy barrier is caused by the breaking of the π–π interactions between the shape-complementary $C_{60}$ and the [10]CPP. In contrast, the translation of the [10]CPP from any position of the aliphatic spacer chain to bind the fullerene is extremely fast, at a timescale of hundreds of nanoseconds, and for this reason, it can be studied simply by classical

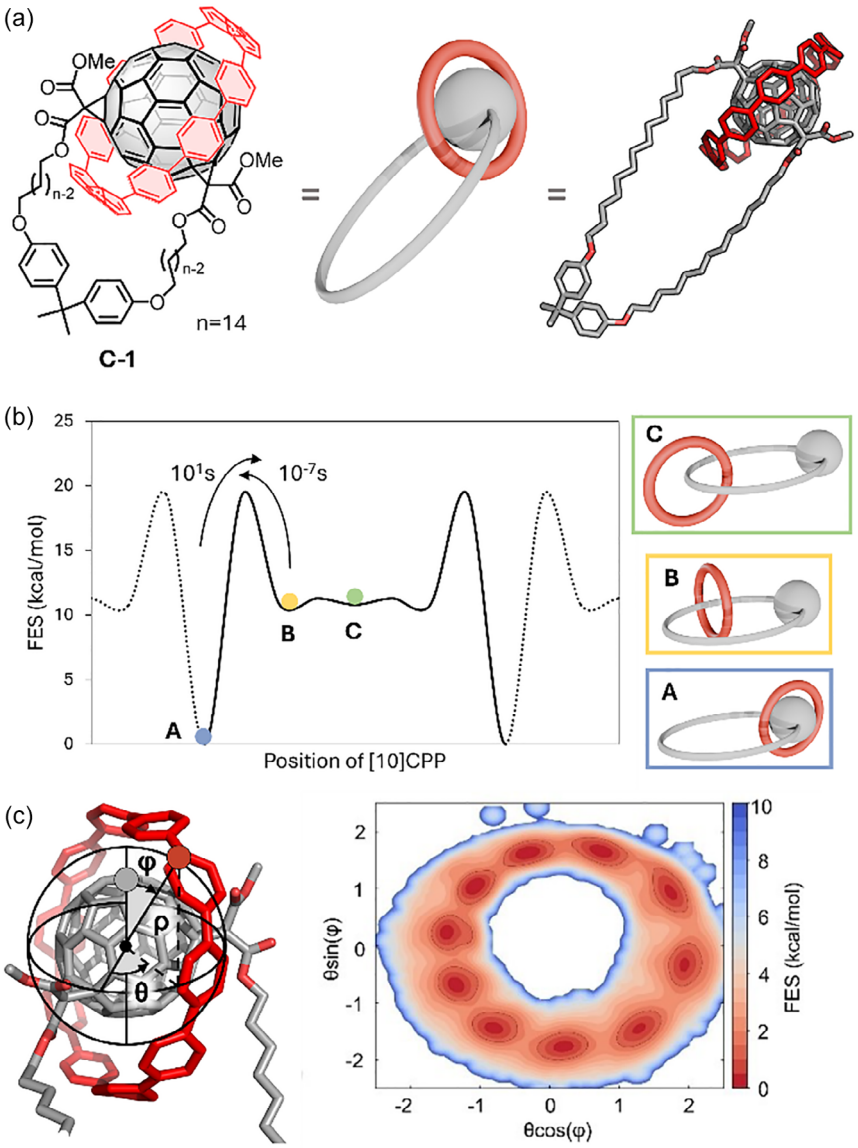


**FIGURE 8** | (a) Structure, schematic representation, and atomistic model of the catenane **C-1** [31]. (b) FES as a function of the position of the [10]CPP with the characteristic transition timescales between each state. (c) Description of the rotation of the [10]CPP around the $C_{60}$ station. FES as a function of the [10]CPP angular configurations ($\theta\cos(\varphi)$ and $\theta\sin(\varphi)$).

MD simulations (Figure 8b). Interestingly, the rotation and tilting of the [10]CPP at the recognition site was also analyzed, observing ten energetically equivalent minima, separated by a small energetic barrier of around ~2 kcal mol$^{-1}$ (Figure 8c), similar to the results obtained for the $C_{60}$-containing rotaxane **R-3** (Figure 6c).

The second example, reported by Steudel et al. in 2025 [32], was specifically designed to test agreement between theory prediction and VT-NMR experiments. To make VT-NMR experiments on shuttling kinetics possible, a catenane architecture with two binding sites and only one ring was pursued (similar to **R-2** and **R-4** discussed above). In a "tour de force" synthesis work, two $C_{60}$ bis-adducts that act as the two recognition sites were connected through relatively rigid chains into a large ring that is mechanically interlocked with the smaller [10]CPP ring (**C-2** in Figure 9a) [32]. As in the previous example, the malonates are nonsymmetric, giving rise to different diastereoisomers. The major product obtained corresponded to the in,in-trans-3 configuration at both fullerenes, resulting in a symmetric [2]catenane **C-2** (with a degenerate binding site). The shuttling of the [10]CPP from one fullerene to the other was investigated by VT-NMR studies, revealing a kinetic barrier of 16.4 kcal mol$^{-1}$. By comparing VT-NMR data for different stereoisomeric catenanes and host–guest complexes, the authors hypothesized that the rigidity of the linker somewhat hinders the exchange motion of the nanohoop. Comparing the experimental data on shuttling (barrier: 16.4 kcal mol$^{-1}$) with the prediction by combined MD/WT-MetaD simulations (barrier: 17.3 kcal mol$^{-1}$) revealed the excellent agreement between experiment and theory, despite the structural complexity of the architecture. Again, the simulations revealed additional insights that are not easily accessible by experiment. In this case, it was found that the [10]CPP ring can also be stabilized at the linker by simultaneously binding the phenyl rings of two different chains (Figure 9b). The process going from one phenyl ring of the linker to the other is considerably fast, occurring at a timescale of around ~16 ns. The binding from this position on the linker to the $C_{60}$ is also fast, with a kinetic barrier of ~9.4 kcal mol$^{-1}$. These results show that shuttling is not limited by diffusion along the axle, but by the initial unbinding of the macrocycle from the recognition site, which is the real rate-limiting step in the shuttling process.

This case is particularly important because the simulations were predictive rather than merely interpretative. The subsequent agreement with VT-NMR experiments shows that, when the relevant transition can be described by appropriate CVs, metadynamics can provide quantitative kinetic predictions even for complex MIM architectures. In fact, it is worth noting that estimating such high free energy barriers at the atomistic level is not easy. Large barriers can typically be accompanied by hidden metastable states that can easily compromise a correct estimation of the barrier and kinetics. The fact that good agreement is obtained here even for such high barriers and with a low number of CVs suggests that these barriers, although high, are relatively simple and neat. This again reinforces the idea that MetaD simulations are well-suited to study MIMs and that, at the same time, MIMs are perfect case studies for MetaD. This also suggests that this type of simulation is not only useful for obtaining deep insights into the factors that control the dynamics of MIMs, but also for their predictive power, which makes them a fundamental tool toward the rational design of MIMs with controllable dynamical behaviors.

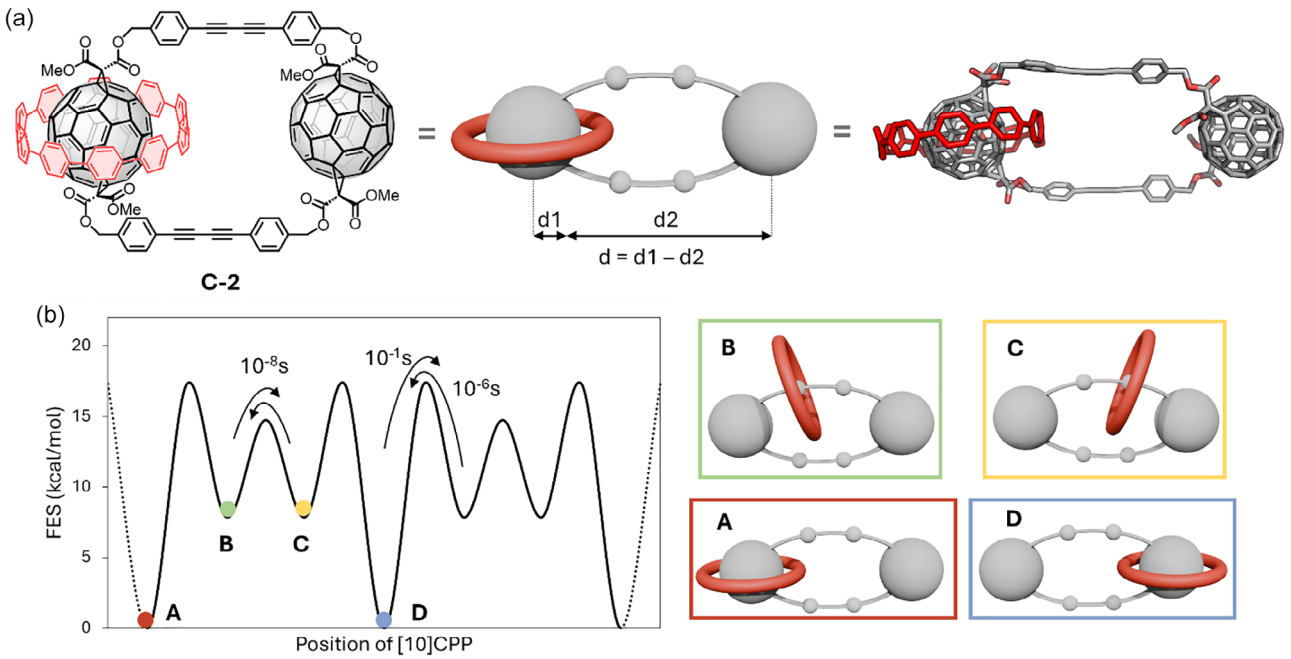


**FIGURE 9** | (a) Structure, schematic representation, and atomistic model of the catenane **C-2** [32]. Description of the CV: *d* being the difference in distance between the center of masses of the [10]CPP (in red) and each $C_{60}$ recognition site. (b) FES as a function of the position of the [10]CPP with the characteristic transition timescales between each state.

## 4.2 | [3]catenane

In general [3], catenanes are challenging to synthesize, so the examples reported to date in the literature are scarce. Thanks to ingenious "ring-in-ring template" design, the synthesis and dynamic studies of an ABC-type hetero [3]catenane were recently reported by Shi et al. in 2025 (**C-3**) (Figure 10a) [33]. The catenane is formed by three different components: a flexible 24-crown-8 as the inner ring, a rigid [12]CPP macrocycle, and a flexible dibenzylammonium thread. The "ring-in-ring template" approach means that the dibenzylammonium promotes the secondary interactions between [12]CPP and 24-crown-8, resulting in the formation of the [3]catenane **C-3**. This molecule features diverse noncovalent interactions, including C–H···π interactions between the 24-crown-8 and the aromatic rings of the [12]CPP and hydrogen bonds between the 24-crown-8 and the dibenzylammonium component. Experimentally, it was not possible to characterize the dynamic motion due to limitations related to the experimental conditions and the complexity of the molecule. This case further highlights the value of molecular simulations for resolving complex motions that remain difficult to characterize experimentally.

In this case, a combination of classical MD and WT-MetaD simulations was needed to sample the different dynamic degrees of freedom (motion modes) present in the [3]catenane **C-3** and their thermodynamics and kinetics. If the dibenzylammonium ring (in blue) is considered as fixed and the protonated station as a recognition site for the [12]CPP (in red) and the 24-crown-8 (in gray), it can be distinguished: the unbinding of the [12]CPP from the 24-crown-8 and the unbinding of the 24-crown-8 from the protonated site of the dibenzylammonium. The characteristic time of the [12]CPP unbinding from the 24-crown-8 was determined to be around 10 μs (Figure 10b). The unbinding of the 24-crown-8 from the recognition site of the dibenzylammonium has a characteristic time of around ~120 μs (Figure 10b). This shows that the diffusion of the crown along the dibenzylammonium thread is one order of magnitude slower than the separation of the crown from the [12]CPP, meaning that the [12]CPP and the crown diffuse separately along the dibenzylammonium thread. Another important motion to consider in [3]catenanes is the rotation of the different macrocycles around themselves. Usually, these motions are relatively fast and can be studied using classical MD simulations, as seen in previous systems, such as [2]catenanes and rotaxanes. In this case study, the [12]CPP nanohoop and the 24-crown-8 ring can freely rotate and tilt (Figure 10c). This analysis suggests that the different components are not transported as a single rigid unit but display partially independent motions on distinct timescales.

## 5 | Summary and Outlook

The combination of MD and MetaD simulations has recently proven to be a powerful and versatile approach to study the dynamics of MIM systems such as rotaxanes and catenanes. The kinetic rates of shuttling and of the different thermally-activated transitions involved in these molecules are often difficult to determine experimentally. For this reason, it is important to develop a computational procedure enabling their estimation. The timescales at which these dynamics occur are often not accessible to unbiased MD simulations, and for this reason, enhanced-sampling approaches become necessary. WT-MetaD allows the reconstruction of the relevant free-energy profiles, while infrequent MetaD simulations enable the estimation of free energy barriers and the associated transition times. In the cases where shuttling has been measured experimentally, the agreement between computed and experimental results supports the precision and therefore utility of these methods. Across the systems discussed here, a recurring feature is that the kinetics of shuttling are governed by the unbinding step from the recognition site, whereas diffusion and local rearrangements are substantially faster. The simulations show that shuttling kinetics are shaped not only by the strength of the recognition sites but also by the flexibility of the components, the presence of intermediate states, and the availability of alternative binding configurations.

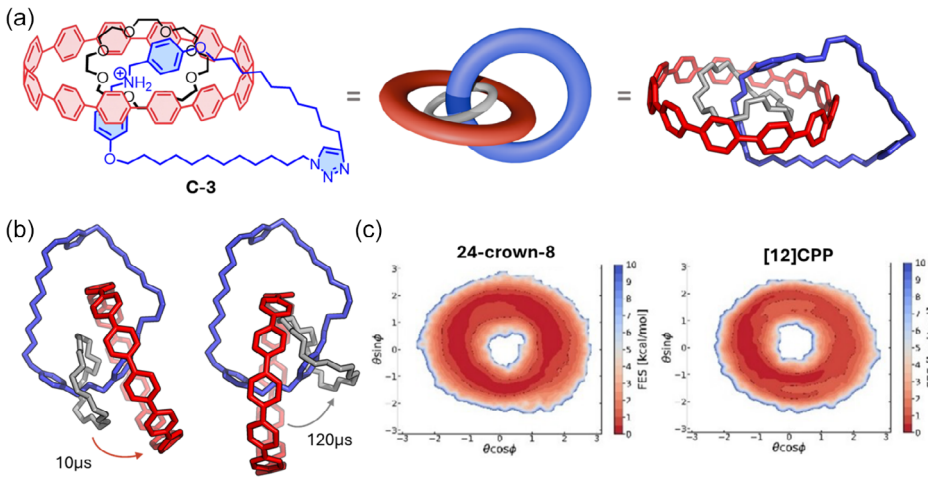


**FIGURE 10** | (a) Structure, schematic representation, and atomistic model of the catenane **C-3** [33]. (b) Representation of the [12]CPP unbinding (in red, on the left) and of the 24-crown-8 (in gray, on the right) with the characteristic transition timescales. (c) FES of the rotation for the 24-crown-8 (on the left) and the [12]CPP (on the right) as a function of the angular configurations ($\theta\cos(\varphi)$ and $\theta\sin(\varphi)$). Reproduced with permission from W. Shi, Y. Hu, L. Leanza et al., Copyright 2025 Wiley-VCH GmbH.

External conditions are also fundamental for the dynamics of MIMs. The solvent, for example, can affect shuttling kinetics in a rotaxane by competing with the macrocycle for hydrogen-bonding interactions with the recognition site.

This MD/WT-MetaD approach performs particularly well for MIMs containing at least one relatively rigid component, where the shuttling process can be effectively described using a low-dimensional CV. However, important limitations arise when all components of the MIM are highly flexible. In these cases, the shuttling mechanism is no longer governed by a single dominant coordinate, but instead involves a complex coupling between translational motion, conformational rearrangements, and entropic contributions. As a result, a single CV is generally insufficient to capture the full transition kinetics and free-energy landscape accurately. This is an important aspect to take into account when applying this MD/WT-MetaD approach.

Although the dynamic transitions discussed throughout this account are generally well described by classical atomistic force fields, future developments are expected to increasingly integrate quantum mechanical descriptions with enhanced sampling techniques. In particular, ab initio and QM/MM metadynamics may provide valuable insight into molecular machines especially when their function is controlled by chemical reactions, proton or electron transfer, photoresponsive units, or other processes in which electronic structure changes play a decisive role. Furthermore, recent advances in machine-learning interatomic potentials offer a promising route to combine near-quantum accuracy with the computational efficiency required to investigate complex free-energy landscapes. These developments are expected to further expand the applicability of enhanced sampling methods to increasingly sophisticated MIMs.

In light of the continued emergence of MIMs with extraordinary functional properties [103–105], we expect that MD and MetaD simulations of MIMs will gain further momentum in the years to come. At the same time, we see potential for gaining deeper insights into the dynamics of other complex supramolecular systems, such as multishell (Matryoshka-type) or oligomeric MIM assemblies.


### Acknowledgments

We thank MCIN Spain (PID2022-136970NB-I00 and TED2021-130573B-I00 to X.R., RYC2020-029552-I, and PID2022-141676NB-I00 to F.F.) and Generalitat de Catalunya (2021SGR00475, 2021SGR00487). C.S. thanks UdG for IF PhD grants. X.R. thanks an ICREA-Academia award. M.v.D. acknowledges support by the Deutsche Forschungsgemeinschaft (DFG) under project numbers 182849149-SFB953 "Synthetic Carbon Allotropes," 445471097, 445470598, and 364549901. M.v.D. and G.M.P. acknowledge funding received by the ERC under the European Union's Horizon 2020 research and innovation program (grant agreements nos. 802428—SUPRANET and 818776—DYNAPOL).


### Conflicts of Interest

The authors declare no conflicts of interest.

### Data Availability Statement

Complete data and materials about the molecular simulations conducted (input files, model files, raw data, analysis, etc.) are available at: https://doi.org/10.5281/zenodo.7991732 (for all rotaxanes), https://doi.org/10.5281/zenodo.8319349 (for **C-1**), https://doi.org/10.5281/zenodo.17093025 (for **C-2**), and https://doi.org/10.5281/zenodo.14655924 (for **C-3**).

### References


1. I. T. Harrison and S. Harrison, "Synthesis of a Stable Complex of a Macrocycle and a Threaded Chain," *Journal of the American Chemical Society* 89 (1967): 5723–5724.

2. E. Wasserman, "The Preparation of Interlocking Rings: A Catenane[1]," *Journal of the American Chemical Society* 82 (1960): 4433–4434.

3. G. Schill and A. Lüttringhaus, "The Preparation of Catena Compounds by Directed Synthesis," *Angewandte Chemie International Edition in English* 3 (1964): 546–547.

4. C. J. Bruns and J. F. Stoddart, *The Nature of the Mechanical Bond: From Molecules to Machines* (2016).

5. Z. Yu, M. Centola, J. Valero, M. Matthies, P. Šulc, and M. Famulok, "A Self-Regulating DNA Rotaxane Linear Actuator Driven by Chemical Energy," *Journal of the American Chemical Society* 143 (2021): 13292–13298.

6. C. J. Bruns and J. F. Stoddart, "Rotaxane-Based Molecular Muscles," *Accounts of Chemical Research* 47 (2014): 2186–2199.

7. S. Erbas-Cakmak, D. A. Leigh, C. T. McTernan, and A. L. Nussbaumer, "Artificial Molecular Machines," *Chemical Reviews* 115 (2015): 10081–10206.

8. M. Baroncini, S. Silvi, and A. Credi, "Photo- and Redox-Driven Artificial Molecular Motors," *Chemical Reviews* 120 (2020): 200–268.

9. A. Coskun, M. Banaszak, R. D. Astumian, J. F. Stoddart, and B. A. Grzybowski, "Great Expectations: Can Artificial Molecular Machines Deliver on Their Promise?," *Chemical Society Reviews* 41 (2012): 19–30.

10. W. Yang, Y. Li, H. Liu, L. Chi, and Y. Li, "Design and Assembly of Rotaxane-Based Molecular Switches and Machines," *Small* 8 (2012): 504–516.

11. E. R. Kay and D. A. Leigh, "Beyond Switches: Rotaxane- and Catenane-Based Synthetic Molecular Motors," *Pure and Applied Chemistry. Chimie Pure Et Appliquee* 80 (2008): 17–29.

12. L. Zhang, H. Wu, X. Li, H. Chen, R. D. Astumian, and J. F. Stoddart, "Artificial Molecular Pumps," *Nature Reviews Methods Primers* 4 (2024): 13.

13. E. Moulin, L. Faour, C. C. Carmona-Vargas, and N. Giuseppone, "From Molecular Machines to Stimuli-Responsive Materials," *Advanced Materials* 32 (2020): 1906036.

14. D. A. Leigh, V. Marcos, and M. R. Wilson, "Rotaxane Catalysts," *ACS Catalysis* 4 (2014): 4490–4497.

15. M. J. Langton and P. D. Beer, "Rotaxane and Catenane Host Structures for Sensing Charged Guest Species," *Accounts of Chemical Research* 47 (2014): 1935–1949.

16. W. Sima, Y. Mai, P. Sun, et al., "Decoupling Thermal Stability and High-Temperature Energy Storage in Polymer Dielectrics via Mechanically Interlocked Supramolecular Structures," *Energy Storage Materials* 84 (2026): 104833.

17. D. A. Leigh, P. J. Lusby, R. T. McBurney, et al., "Getting Harder: Cobalt(III)-Template Synthesis of Catenanes and Rotaxanes," *Journal of the American Chemical Society* 131 (2009): 3762–3771.

18. V. Aucagne, J. Berná, J. D. Crowley, et al., "Catalytic "Active-Metal" Template Synthesis of [2]Rotaxanes, [3]Rotaxanes, and Molecular Shuttles, and Some Observations on the Mechanism of the Cu(I)-

Catalyzed Azide–Alkyne 1,3-Cycloaddition," *Journal of the American Chemical Society* 129 (2007): 11950–11963.

19. G. Gholami, K. Zhu, G. Baggi, E. Schott, X. Zarate, and S. J. Loeb, "Influence of Axle Length on the Rate and Mechanism of Shuttling in Rigid H-Shaped [2]rotaxanes," *Chemical Science* 8 (2017): 7718–7723.

20. J. Puigcerver, M. Alajarin, A. Martinez-Cuezva, and J. Berna, "Modulating the Shuttling Motion of [2]rotaxanes Built of *p* - Xylylenediamine Units through Permethylation at the Benzylic Positions of the ring," *Organic & Biomolecular Chemistry* 21 (2023): 9070–9075.

21. S.-Y. Chang, J. S. Choi, and K.-S. Jeong, "Self-Assembly and Dynamics of [2]- and [3]Rotaxanes with a Dinuclear Macrocycle Containing Reversible Os–N Coordinate Bonds," *Chemistry - A European Journal* 7 (2001): 2687–2697.

22. N. Bukhtiiarova, A. Credi, and S. Corra, "Controlling Molecular Shuttling in a Rotaxane with Weak ring Recognition Sites," *Chemical Communications* 59 (2023): 13159–13162.

23. G. Fioravanti, N. Haraszkiewicz, E. R. Kay, et al., "Three State Redox-Active Molecular Shuttle That Switches in Solution and on a Surface," *Journal of the American Chemical Society* 130 (2008): 2593–2601.

24. M. R. Panman, P. Bodis, D. J. Shaw, et al., "Operation Mechanism of a Molecular Machine Revealed Using Time-Resolved Vibrational Spectroscopy," *Science* 328 (2010): 1255–1258.

25. T. Nicolás-García, N. Martín Sabanés, R. Bocanegra, R. D. Astumian, E. M. Pérez, and B. Ibarra, "Transition-Path Times of Individual Molecular Shuttles under Mechanical Equilibrium Show Symmetry," *Chem* 11 (2025): 102410.

26. T. Naranjo, K. M. Lemishko, S. de Lorenzo, et al., "Dynamics of Individual Molecular Shuttles under Mechanical Force," *Nature Communications* 9 (2018): 4512.

27. B. Brough, B. H. Northrop, J. J. Schmidt, et al., "Evaluation of Synthetic Linear Motor-Molecule Actuation Energetics," *Proceedings of the National Academy of Sciences* 103 (2006): 8583–8588.

28. L. Leanza, C. Perego, L. Pesce, M. Salvalaglio, M. von Delius, and G. M. Pavan, "Into the Dynamics of Rotaxanes at Atomistic Resolution," *Chemical Science* 14 (2023): 6716–6729.

29. X. Grabuleda, P. Ivanov, and C. Jaime, "Shuttling Process in [2]Rotaxanes. Modeling by Molecular Dynamics and Free Energy Perturbation Simulations," *The Journal of Physical Chemistry B* 107 (2003): 7582–7588.

30. G. Jana and J. L. Mendoza-Cortes, "Thermodynamics, Kinetics, and Optical Properties of Rotaxane: A First-Principles Molecular Dynamics Study," *The Journal of Physical Chemistry A* 127 (2023): 2671–2687.

31. F. M. Steudel, E. Ubasart, L. Leanza, et al., "Synthese von C60/[10] CPP-Catenanen durch Regioselektive Nanokapsel-Templierte Bingel Bis-Addition," *Angewandte Chemie International Edition* 135 (2023): 62.

32. F. M. Steudel, C. Sabria, M. D. Piane, et al., "Observation of Shuttling On the One-second Timescale in a [10] Cycloparaphenylene/C60 [2] Catenane," *Chemical Science* 16 (2025): 21908.

33. W. Shi, Y. Hu, L. Leanza, et al., "Ring-in-Ring Assembly Facilitates the Synthesis of a [12]Cycloparaphenylene ABC-Type [3]Catenane," *Angewandte Chemie International Edition* 64 (2025): e202421459.

34. A. R. Leach, *Molecular Modelling: Principles and Applications* (Pearson education, 2001).

35. J. D. Durrant and J. A. McCammon, "Molecular Dynamics Simulations and Drug Discovery," *BMC Biology* 9 (2011): 71.

36. F. Feixas, S. Lindert, W. Sinko, and J. A. McCammon, "Exploring the Role of Receptor Flexibility in Structure-Based Drug Discovery," *Biophysical Chemistry* 186 (2014): 31–45.

37. M. G. Pikkemaat, A. B. M. Linssen, H. J. C. Berendsen, and D. B. Janssen, "Molecular Dynamics Simulations as a Tool for Improving Protein Stability," *Protein Engineering* 15 (2002): 185–192.

38. S. Sinha, B. Tam, and S. M. Wang, "Applications of Molecular Dynamics Simulation in Protein Study," *Membranes* 12 (2022): 844.

39. M. Karplus and J. A. McCammon, "Molecular Dynamics Simulations of Biomolecules," *Nature Structural Biology* 9 (2002): 646–652.

40. Y. Miao, F. Feixas, C. Eun, and J. A. McCammon, "Accelerated Molecular Dynamics Simulations of Protein Folding," *Journal of Computational Chemistry* 36 (2015): 1536–1549.

41. P. J. Bond, J. M. Cuthbertson, S. S. Deol, and M. S. P. Sansom, "MD Simulations of Spontaneous Membrane Protein/Detergent Micelle Formation," *Journal of the American Chemical Society* 126 (2004): 15948–15949.

42. H. Hata, M. Nishiyama, and A. Kitao, "Molecular Dynamics Simulation of Proteins under High Pressure: Structure, Function and Thermodynamics," *Biochimica et Biophysica Acta (BBA) - General Subjects* 1864 (2020): 129395.

43. J. J. Prompers and R. Brüschweiler, "General Framework for Studying the Dynamics of Folded and Nonfolded Proteins by NMR Relaxation Spectroscopy and MD Simulation," *Journal of the American Chemical Society* 124 (2002): 4522–4534.

44. L. Pesce, C. Perego, A. B. Grommet, R. Klajn, and G. M. Pavan, "Molecular Factors Controlling the Isomerization of Azobenzenes in the Cavity of a Flexible Coordination Cage," *Journal of the American Chemical Society* 142 (2020): 9792–9802.

45. C. García-Simón, C. Colomban, Y. A. Çetin, et al., "Complete Dynamic Reconstruction of $C_{60}$, $C_{70}$, and $(C_{59}\ N)_2$ Encapsulation into an Adaptable Supramolecular Nanocapsule," *Journal of the American Chemical Society* 142 (2020): 16051–16063.

46. R. Choudhury, A. Barman, R. Prabhakar, and V. Ramamurthy, "Hydrocarbons Depending on the Chain Length and Head Group Adopt Different Conformations Within a Water-Soluble Nanocapsule: $^1$H NMR and Molecular Dynamics Studies," *The Journal of Physical Chemistry B* 117 (2013): 398–407.

47. M. Kirca, "Design and Analysis of Sandwiched Fullerene-Graphene Composites Using Molecular Dynamics Simulations," *Composites. Part B, Engineering* 79 (2015): 513–520.

48. A. H. Mazurek, Ł. Szeleszczuk, and T. Gubica, "Application of Molecular Dynamics Simulations in the Analysis of Cyclodextrin Complexes," *International Journal of Molecular Sciences* 22 (2021): 9422.

49. C. Fuertes-Espinosa, C. García-Simón, M. Pujals, et al., "Supramolecular Fullerene Sponges as Catalytic Masks for Regioselective Functionalization of C60," *Chem* 6 (2020): 169–186.

50. M. Pujals, T. Pèlachs, C. Fuertes-Espinosa, T. Parella, M. Garcia-Borràs, and X. Ribas, "Regioselective Access to Orthogonal Diels-Alder C60 Bis-Adducts and Tris-Heteroadducts via Supramolecular Mask Strategy," *Cell Reports Physical Science* 3 (2022): 100992.

51. O. Shyshov, S. V. Haridas, L. Pesce, et al., "Living Supramolecular Polymerization of Fluorinated Cyclohexanes," *Nature Communications* 12 (2021): 3134.

52. S. Hollstein and M. von Delius, "The Dynamic Chemistry of Orthoesters and Trialkoxysilanes: Making Supramolecular Hosts Adaptive, Fluxional, and Degradable," *Accounts of Chemical Research* 57 (2024): 602–612.

53. S. Patodia, A. Bagaria, and D. Chopra, "Molecular dynamics simulation of proteins: a brief overview," *Journal of Chemical, Biological and Physical Sciences* 4 (2014): 1–4.

54. S. A. Hollingsworth and R. O. Dror, "Molecular Dynamics Simulation for All," *Neuron* 99 (2018): 1129–1143.

55. D. Frenkel and B. Smit, *Understanding Molecular Simulation: From Algorithms to Applications* (Academic Press, 2023).

56. M. A. González, "Force Fields and Molecular Dynamics Simulations," *JDN* 12 (2011): 169–200.

57. J. Behler and M. Parrinello, "Generalized Neural-Network Representation of High-Dimensional Potential-Energy Surfaces," *Physical Review Letters* 98 (2007): 146401.

58. A. P. Bartók, M. C. Payne, R. Kondor, and G. Csányi, "Gaussian Approximation Potentials: The Accuracy of Quantum Mechanics, without the Electrons," *Physical Review Letters* 104 (2010): 136403.

59. J. Zeng, D. Zhang, A. Peng, et al., "DeePMD-Kit v3: A Multiple-Backend Framework for Machine Learning Potentials," *Journal of Chemical Theory and Computation* 21 (2025): 4375–4385.

60. L. Bonati and M. Parrinello, "Silicon Liquid Structure and Crystal Nucleation from *Ab Initio* Deep Metadynamics," *Physical Review Letters* 121 (2018): 265701.

61. J. S. Smith, O. Isayev, and A. E. Roitberg, "ANI-1: an Extensible Neural Network Potential with DFT Accuracy at Force Field Computational Cost," *Chemical Science* 8 (2017): 3192–3203.

62. E. Gelžinytė, M. Öeren, M. D. Segall, and G. Csányi, "Transferable Machine Learning Interatomic Potential For Bond Dissociation Energy Prediction of Drug-like Molecules," *Journal of Chemical Theory and Computation* 20 (2023): 164.

63. I. Batatia, S. Batzner, D. P. Kovács, et al., "The Design Space of E(3)-Equivariant Atom-Centred Interatomic Potentials," *Nature Machine Intelligence* 7 (2025): 56–67.

64. Y. I. Yang, Q. Shao, J. Zhang, L. Yang, and Y. Q. Gao, "Enhanced Sampling in Molecular Dynamics," *The Journal of Chemical Physics* 151 (2019): 7.

65. J. Hénin, T. Lelièvre, M. R. Shirts, and L. D. Omar Valsson, "Enhanced Sampling Methods for Molecular Dynamics Simulations," *Computational Molecular Science* 4 (2022): 1.

66. S. Datta, Y. Kato, S. Higashiharaguchi, et al., "Self-Assembled Poly-Catenanes from Supramolecular Toroidal Building Blocks," *Nature* 583 (2020): 400–405.

67. A. Laio and M. Parrinello, "Escaping Free-Energy Minima," *Proceedings of the National Academy of Sciences* 99 (2002): 12562–12566.

68. P. Tiwary and M. Parrinello, "From Metadynamics to Dynamics," *Physical Review Letters* 111 (2013): 230602.

69. D. Ray and M. Parrinello, "Kinetics from Metadynamics: Principles, Applications, and Outlook," *Journal of Chemical Theory and Computation* 19 (2023): 5649–5670.

70. A. Barducci, M. Bonomi, and M. Parrinello, "Metadynamics," *WIREs Computational Molecular Science* 1 (2011): 826–843.

71. A. Barducci, G. Bussi, and M. Parrinello, "Well-Tempered Metadynamics: A Smoothly Converging and Tunable Free-Energy Method," *Physical Review Letters* 100 (2008): 020603.

72. C. D. Fu, L. F. L. Oliveira, and J. Pfaendtner, "Determining Energy Barriers and Selectivities of a Multi-pathway System With Infrequent Metadynamics," *The Journal of Chemical Physics* 146 (2017): 1.

73. Y. Wang, O. Valsson, P. Tiwary, M. Parrinello, and K. Lindorff-Larsen, "Frequency Adaptive Metadynamics for the Calculation of Rare-event Kinetics," *The Journal of Chemical Physics* 149 (2018): 7.

74. D. Bochicchio, M. Salvalaglio, and G. M. Pavan, "Into the Dynamics of a Supramolecular Polymer at Submolecular Resolution," *Nature Communications* 8 (2017): 147.

75. A. L. de Marco, D. Bochicchio, A. Gardin, G. Doni, and G. M. Pavan, "Controlling Exchange Pathways in Dynamic Supramolecular Polymers by Controlling Defects," *ACS Nano* 15 (2021): 14229–14241.

76. M. Delle Piane, L. Pesce, M. Cioni, and G. M. Pavan, "Reconstructing Reactivity in Dynamic Host–guest Systems at Atomistic Resolution: Amide Hydrolysis under Confinement in the Cavity of a Coordination Cage," *Chemical Science* 13 (2022): 11232–11245.

77. D. Bochicchio, S. Kwangmettatam, T. Kudernac, and G. M. Pavan, "How Defects Control the Out-of-Equilibrium Dissipative Evolution of a Supramolecular Tubule," *ACS Nano* 13 (2019): 4322–4334.

78. C. Lionello, A. Gardin, A. Cardellini, et al., "Toward Chemotactic Supramolecular Nanoparticles: From Autonomous Surface Motion Following Specific Chemical Gradients to Multivalency-Controlled Disassembly," *ACS Nano* 15 (2021): 16149–16161.

79. G. Bussi and A. Laio, "Using Metadynamics to Explore Complex Free-Energy Landscapes," *Nature Reviews Physics* 2 (2020): 200–212.

80. C. Lionello, C. Perego, A. Gardin, R. Klajn, and G. M. Pavan, "Supramolecular Semiconductivity through Emerging Ionic Gates in Ion–Nanoparticle Superlattices," *ACS Nano* 17 (2023): 275–287.

81. R. Capelli and G. Piccini, "Atomistic Insights into Hydrogen-Bonded Supramolecular Capsule Self-Assembly Dynamics," *The Journal of Physical Chemistry C* 128 (2024): 635–641.

82. V. V. Welborn, W.-L. Li, and T. Head-Gordon, "Interplay of Water and a Supramolecular Capsule for Catalysis of Reductive Elimination Reaction from Gold," *Nature Communications* 11 (2020): 415.

83. H. Lambert, A. Castillo Bonillo, Q. Zhu, Y.-W. Zhang, and T.-C. Lee, "Supramolecular Gating of Guest Release from Cucurbit[7]uril Using De Novo Design," *NPJ Computational Materials* 8 (2022): 21.

84. J. Groppi, L. Casimiro, M. Canton, et al., "Precision Molecular Threading/Dethreading," *Angewandte Chemie International Edition* 59 (2020): 14825–14834.

85. G. Tabacchi, S. Silvi, M. Venturi, A. Credi, and E. Fois, "Dethreading of a Photoactive Azobenzene-Containing Molecular Axle from a Crown Ether Ring: A Computational Investigation," *ChemPhysChem* 17 (2016): 1913–1919.

86. K. Gogoi, P. Adhikary, P. K. Matsa, G. Allada, R. Biswas, and S. Chakraborty, "Viologen-Terminated Redox-Active [2] rotaxane Stabilised by Electrostatic Gating," *ChemRxiv* (2026): 2026.

87. S. Ibáñez, M. Alemany-Chavarria, L. N. Dawe, G. Ujaque, and E. Peris, "Rocking (and Shuttling) in a Nanosized Metallobox," *Angewandte Chemie International Edition* 64 (2025): e202514744.

88. M. Hmadeh, A. C. Fahrenbach, S. Basu, et al., "Electrostatic Barriers in Rotaxanes and Pseudorotaxanes," *Chemistry – A European Journal* 17 (2011): 6076–6087.

89. V. Balzani, A. Credi, and M. Venturi, "Light Powered Molecular Machines," *Chemical Society Reviews* 38 (2009): 1542–1550.

90. P. G. Young, K. Hirose, and Y. Tobe, "Axle Length Does Not Affect Switching Dynamics in Degenerate Molecular Shuttles with Rigid Spacers," *Journal of the American Chemical Society* 136 (2014): 7899–7906.

91. O. Borodin, Y. Shchukin, C. C. Robertson, S. Richter, and M. von Delius, "Self-Assembly of Stimuli-Responsive [2]Rotaxanes by Amidinium Exchange," *Journal of the American Chemical Society* 143 (2021): 16448–16457.

92. M. J. Kamlet and R. Taft, "The Solvatochromic Comparison Method. I. The .beta.-Scale of Solvent Hydrogen-Bond Acceptor (HBA) Basicities," *Journal of the American Chemical Society* 98 (1976): 377–383.

93. Y. Xu, R. Kaur, B. Wang, et al., "Concave–Convex π–π Template Approach Enables the Synthesis of [10]Cycloparaphenylene–Fullerene [2]Rotaxanes," *Journal of the American Chemical Society* 140 (2018): 13413–13420.

94. S. Nygaard, K. C. F. Leung, I. Aprahamian, et al., "Functionally Rigid Bistable [2]Rotaxanes," *Journal of the American Chemical Society* 129 (2007): 960–970.

95. G. Gil-Ramírez, D. A. Leigh, and A. J. Stephens, "Catenanes: Fifty Years of Molecular Links," *Angewandte Chemie International Edition* 54 (2015): 6110–6150.

96. Q. Chen and K. Zhu, "Advancements and Strategic Approaches in Catenane Synthesis," *Chemical Society Reviews* 53 (2024): 5677–5703.

97. F. B. L. Cougnon, N. A. Jenkins, G. D. Pantoş, and J. K. M. Sanders, "Templated Dynamic Synthesis of a [3]Catenane," *Angewandte Chemie International Edition* 51 (2012): 1443–1447.

98. J. D. Megiatto Jr. and D. I. Schuster, ""Click" Methodology for Synthesis of Functionalized [3]Catenanes: Toward Higher Interlocked Structures," *Chemistry – A European Journal* 15 (2009): 5444–5448.

99. D. B. Amabilino, P. R. Ashton, A. S. Reder, N. Spencer, and J. F. Stoddart, "Olympiadane," *Angewandte Chemie International Edition in English* 33 (1994): 1286–1290.

100. M. B. Podh, R. Ratha, and C. S. Purohit, "Template Assisted Synthesis of Linear [5] Catenane by Post-Functionalization of Templated [2] Catenane and Using Click Reaction," *Chemistry–An Asian Journal* 19 (2024): e202400351.

101. A. W. H. Ng, S. K.-M. Lai, C.-C. Yee, and H. Y. Au-Yeung, "Macrocycle Dynamics in a Branched [8]Catenane Controlled by Three Different Stimuli in Three Different Regions," *Angewandte Chemie International Edition* 61 (2022): e202110200.

102. Q. Wu, P. M. Rauscher, X. Lang, et al., "Poly[*n*]catenanes: Synthesis of Molecular Interlocked Chains," *Science* 358 (2017): 1434–1439.

103. M. I. Bardot, C. W. Weyhrich, Z. Shi, et al., "Mechanically Interlocked Two-Dimensional Polymers," *Science* 387 (2025): 264–269.

104. Y. Gao, P. Gupta, I. Rončević, et al., "Solution-Phase Stabilization of a Cyclocarbon by Catenane Formation," *Science* 389 (2025): 708–710.

105. M Müßler, M. Semwal, K. P. Zois, et al., "Photocatalytically Active Rotaxane Mimicking Photosystem I," *ChemRxiv* (2025): 2025.

## Biographies

**Clara Sabrià** (1998, Girona) obtained her master's degree in Chemistry from the University of Girona (UdG) in 2021, where she was centred on using molecular dynamics (MD) simulations to study the encapsulation of fullerenes in supramolecular cages. She is currently a Ph.D. student at UdG, where her research focuses on the study of different supramolecular systems, using experimental and computational techniques.

**Luigi Leanza** (1995, Bronte) obtained his Ph.D. in materials science and technology from the Polytechnic University of Turin in 2023, where his research focused on the application of classical molecular dynamics, enhanced sampling techniques, and multiscale modeling to supramolecular systems. He spent nearly two years as a postdoctoral researcher in Giovanni Pavan's group, continuing this line of research. He is currently an R&D engineer at Nextmol in Barcelona.

**Massimo Delle Piane** (1986, Torino) obtained his Ph.D. in chemical and material sciences from the University of Torino. He spent nearly five years at the Bremen Center for Computational Materials Science, working on atomic-scale processes in complex materials, and joined Politecnico di Torino (Department of Applied Science and Technology) in 2020, where he is currently associate professor in physics. His research focuses on computational condensed matter physics, multiscale simulations, machine-learning approaches, and structure–spectra relationships to study surfaces, defects, interfaces, and complex molecular and materials systems.

**Max von Delius** (1982, Nurnberg) is professor of organic chemistry at Ulm University (Germany). He obtained his Ph.D. at the University of Edinburgh and was a postdoctoral fellow at the University of Toronto, before establishing his independent research group at FAU Erlangen-Nürnberg (Germany) in 2013. His research interests include supramolecular chemistry, systems chemistry, and the synthesis of functional organic materials. He has been awarded an ERC Starting Grant and has received the Cram-Lehn-Pedersen Prize.

**Ferran Feixas** (1983, Banyoles) obtained his Ph.D. in chemistry from the University of Girona (UdG) in 2011. He then carried out a two-year postdoctoral stay at the University of California San Diego (UCSD), where he worked on biomolecular simulations and enhanced sampling methods. In 2015, he returned to UdG with a Marie Curie Individual Fellowship, and subsequently, he obtained a Ramón y Cajal research position. His research currently focuses on the development and application of computational protocols to study biochemical and supramolecular processes.

**Xavi Ribas** (1974, Santa Coloma de Farners) obtained his Ph.D. in chemistry from the University of Girona (UdG) in 2001, and he carried out a 3-year postdoc at ICMAB-CSIC in 2002–2004. He was promoted to associate professor in Chemistry at UdG in 2006 and to full professor in 2022. He received an ERC-StG project in 2011, several ICREA-Academia Award (2010, 2015, and 2020), and the Excellence in Research Award from RSEQ in 2018. His research currently focuses on the development of nanocages for catalysis and fullerene regiofunctionalization with supramolecular masks.

**Giovanni M. Pavan** (1981, Pordenone) earned his Ph.D. in nanotechnology from the University of Trieste (IT) in 2010. Between 2010-2018 he conducted his research at SUPSI (University of Applied Sciences and Arts of Southern Switzerland), first as a postdoc, then as tenured and senior researcher. In 2019, he founded and led the Computational Materials Science (CMS) laboratory of SUPSI. Since 2019 he has been full professor of physical-chemistry at Politecnico di Torino, where he leads the Computational Physics and Chemistry (CPC) Laboratory. He has coauthored about 150 peer reviewed publications that appeared in high-impact scientific journals and received major national and international funding grants (e.g., ERC, H2020, SNSF, etc.).